Improving Accuracy in Estimation of Artery-Wall Displacement by Referring to Center Frequency of RF Echo

Hideyuki Hasegawa, *Member, IEEE*, and Hiroshi Kanai, *Member, IEEE*

Abstract—Noninvasive measurement of mechanical properties, such as elasticity, of the arterial wall, is useful for diagnosis of atherosclerosis. The elasticity of the arterial wall can be estimated by combining measurement of displacement of the arterial wall with that of blood pressure. In general, the displacement of the arterial wall is estimated from the phase shift of radio frequency (RF) echoes between two consecutive frames using a correlation estimator with quadrature demodulated complex signals. Recently, digitized data of broadband RF echoes are available in modern diagnostic equipment. The Fourier transform can be used to estimate the phase of the RF echo at each frequency within the RF frequency bandwidth. Therefore, the phase shifts between RF echoes of two consecutive frames can be estimated at multiple frequencies. In this estimation, due to object displacement, the RF echo is time shifted in comparison with that of the previous frame. However, the position of the time window for the Fourier transform is not changed between two consecutive frames. This change in relative position between the RF echo and the time window has a strong influence on the estimation of the artery-wall displacement, resulting in error. To suppress this error, the phase shift should be estimated at the actual RF center frequency. In this paper, this error suppression was investigated through simulation experiments and in vivo experiments on the human carotid artery.

I. Introduction

NONINVASIVE measurement of mechanical properties of the arterial wall, such as elasticity, is useful for diagnosing atherosclerosis because there are significant differences between the elastic moduli of normal arterial walls and those affected by atherosclerosis [1], [2].

For assessment of mechanical properties, various methods have been proposed to measure the displacement of the arterial wall. Elasticity, based on estimation of the pulse wave velocity (PWV) [3]–[6], and homogeneity of distensibility [7], which is evaluated by using the change in diameter obtained from displacements of the near and far walls, are noninvasively evaluated by measuring displacements at multiple points along the axial direction of the artery. By definition, one-point measurement of the change in diameter is widely used for assessment of mechanical properties of the arterial wall [8]–[10].

In addition to the displacement distribution in the axial direction of the artery, the distribution in the radial direction of the arterial wall has been measured with intravascular ultrasonography (IVUS) [11], [12]. In the cited studies, the elasticity distribution of coronary atherosclerotic plaque was obtained by the measured displacement distribution in the radial direction. Comparison of such measured elasticity distribution with the pathological image suggested the potential for tissue characterization of atherosclerotic plaque by measuring its elasticity.

As a transcutaneous approach, the displacement and strain around carotid atherosclerotic plaque have been measured using tissue Doppler imaging [13]. The inhomogeneity in displacements measured upstream and downstream of atherosclerotic plaque suggested that artery-wall motion has potential for use in the evaluation of plaque vulnerability.

We have been measuring the displacement and change in thickness of the arterial wall caused by the heartbeat with transcutaneous ultrasound [14]–[16]. Elasticity images of the human carotid artery have been obtained by the measured displacement distribution, and the novel potential for transcutaneous tissue characterization has been shown by classifying the elasticity images using the elasticity reference data obtained by in vitro experiments [17], [18].

In the various methods described above, an autocorrelation technique [19] is widely used for measurement of velocities of blood flow and tissue motion. This technique was designed to estimate the phase shift, $\Delta\theta(f_0)$, with respect to the center frequency, f_0, of a radio frequency (RF) echo using a complex signal, $\check{rf}(t)$, which is obtained by quadrature demodulation at a demodulation frequency, f_{dem}. Therefore, use of a conventional autocorrelator requires knowledge of the actual center frequency, f_0, of an RF echo to obtain unbiased velocity estimates. To overcome this problem, both the mean phase shift, $\Delta\theta(f_0)$, and the RF center frequency, f_0, are estimated by applying the two-dimensional (2-D) [time (depth)–frame] Fourier transform to RF echoes, $rf_1(t)$ and $rf_2(t)$, of two consecutive frames [20]. However, an autocorrelation technique with the quadrature demodulated complex signal, $\check{rf}(t)$, would be preferable because autocorrelation methods require lower sampling frequency in comparison with the analysis of RF echoes. Therefore, use of a 2-D [time (depth)–frame] autocorrelator with quadrature demodulated signals, $\check{rf}(t)$, has been proposed to estimate the mean

Doppler frequency and the RF center frequency. Estimation by the 2-D autocorrelator has been proven to be identical to that with the 2-D Fourier transform [21]. A 2-D autocorrelator recently was applied to the measurement of vessel wall displacement [22].

Recently, digitized data of broadband RF echoes have become available in modern diagnostic equipment. For velocity (displacement) estimation, the Fourier transform can be used to extract the phase information of RF echoes at multiple frequencies within the frequency bandwidth of an RF echo. In the phase-shift estimation with the Fourier transform, the position of the time window for the Fourier transform relative to an RF echo changes frame by frame due to object displacement. Such a change in relative position influences the estimated phase shift of the RF echo at frequencies other than the RF center frequency. In the present study, this problem was investigated through simulation experiments and in vivo experiments on the human carotid artery.

II. METHODS

A. Velocity Estimation from the Phase Shift of RF Echoes with Wall Tracking

Let us define the time series and the frequency spectrum of the transmitted ultrasonic pulse by $s(t)$ and $S(f)$, respectively. The received RF echo has a specific time delay depending on the distance between the ultrasonic probe and the object. When the object is displaced, time delays of RF echoes measured at two consecutive frames differ. By defining time delays at the n-th and $(n+1)$-th frames $(n = 1, 2, \ldots, N-1)$ by τ_n and τ_{n+1}, received RF echoes at the n-th and $(n+1)$-th frames are expressed as $s(t-\tau_n)$ and $s(t-\tau_{n+1})$, respectively. The frequency spectra of $s(t-\tau_n)$ and $s(t-\tau_{n+1})$ are obtained by applying the Fourier transform, FT[·], as follows:

$$\widehat{S_n}(f) \equiv \mathrm{FT}[s(t - \tau_n)] = S(f) \cdot e^{-j2\pi f \tau_n}, \tag{1}$$

$$\widehat{S_{n+1}}(f) \equiv \mathrm{FT}[s(t - \tau_{n+1})] = S(f) \cdot e^{-j2\pi f \tau_{n+1}}. \tag{2}$$

Therefore, the change in time delay, $\tau_{n+1} - \tau_n$, which corresponds to the object displacement between the n-th and $(n + 1)$-th frames, can be estimated from the phase, $\Delta\theta_n(f)$, of the cross-spectrum, $S_n^*(f) \cdot S_{n+1}(f)$, at a frequency, f, as follows:

$$\widehat{S_n}^*(f) \cdot \widehat{S_{n+1}}(f) = |\widehat{S_n}(f)||\widehat{S_{n+1}}(f)| \cdot e^{j\widehat{\Delta\theta_n}(f)}$$
$$= |S(f)|^2 \cdot e^{-j2\pi f(\tau_{n+1} - \tau_n)}, \tag{3}$$

where $*$ represents the complex conjugate.

By defining the sound speed as c_0, distances d_n and d_{n+1} between the ultrasonic probe and the object at n-th and $(n + 1)$-th frames are given by:

$$d_n = \frac{c_0 \tau_n}{2}, \tag{4}$$

$$d_{n+1} = \frac{c_0 \tau_{n+1}}{2}. \tag{5}$$

Describing object displacement between the n-th and $(n+1)$-th frames by $\Delta d_n = d_{n+1} - d_n$, object displacement, Δd_n, between two consecutive frames is obtained from the phase shift, $\widehat{\Delta\theta_n}(f)$, at a frequency, f, estimated by (3) as follows:

$$\widehat{\Delta d_n} = d_{n+1} - d_n = \frac{c_0(\tau_{n+1} - \tau_n)}{2} = -\frac{c_0 \cdot \widehat{\Delta\theta_n}(f)}{4\pi f}. \tag{6}$$

From the estimated displacement, $\widehat{\Delta d_n}$, between two consecutive frames, the velocity of the object is obtained using the frame interval, T, as follows:

$$\widehat{v_n} = \frac{\widehat{\Delta d_n}}{T} = -\frac{c_0 \cdot \widehat{\Delta\theta_n}(f)}{4\pi f T}. \tag{7}$$

In this process, the wall position, d_n, is tracked by integrating the estimated velocity, v_n, as follows [14]:

$$\widehat{d_{n+1}} = d_0 + \sum_{1}^{n} \widehat{v_n} \cdot T, \tag{8}$$

where d_0 is the initial wall position manually assigned at the initial frame.

B. Principle for Simulating RF Echoes

Fig. 1 illustrates the time shift of the RF echo due to object displacement. When a short time window is used to obtain the phase of the received signal, a portion of the duration in the period shown by the region with oblique lines is excluded due to the time shift of the RF echo caused by object displacement. This change in the relative position between the echo and the time window causes an error in estimation of the time shift of the RF echo. In this study, the error caused by the change in relative position between the echo and the time window was investigated using RF echoes simulated in the following way. A digitized ultrasonic RF echo, $\mathrm{rf}_n(m)$, from an interface or a point scatterer of the n-th frame at a time $t = mT_s$ $(m = 1, 2, 3, \ldots;$ T_s: sampling interval) is defined by a sinusoidal wave at a center angular frequency of $\omega_0 = 2\pi f_0$ and an envelope, $\mathrm{env}_n(m)$, as shown in (9) and (10) (see next page), where ΔT_p and τ_n are the pulse length and the time delay at the n-th frame, respectively. In the simulation experiments, τ_n is defined as the time delay from the beginning of the time window as shown in Fig. 1. The time delay, τ_n, differs frame by frame when the object is displaced.

The change in time delay, $\tau_{n+1} - \tau_n$, between two neighboring frames is estimated based on (3) by applying the discrete Fourier transform to $\mathrm{rf}_n(m)$ and $\mathrm{rf}_{n+1}(m)$.

A very simple model was used in the present study because in cases of arterial walls without atherosclerotic plaque, echoes can be modeled by such a simple model

$$\mathrm{rf}_n(m) = \mathrm{env}_n(m) \cdot \sin\left\{\omega_0(mT_s - \tau_n)\right\} = \mathrm{env}_n(m) \cdot \frac{e^{j\omega_0(mT_s-\tau_n)} - e^{-j\omega_0(mT_s-\tau_n)}}{2j}, \tag{9}$$

$$\mathrm{env}_n(m) = \begin{cases} \sin^2\left\{\pi\dfrac{mT_s-\tau_n}{\Delta T_p}\right\} = 0.5\left\{1 - \dfrac{e^{j2\pi\frac{mT_s-\tau_n}{\Delta T_p}} + e^{-j2\pi\frac{mT_s-\tau_n}{\Delta T_p}}}{2}\right\} \\ \qquad\qquad\qquad\qquad (\tau_n \le mT_s \le \tau_n + \Delta T_p), \\ 0\ (mT_s < \tau_n,\ mT_s > \tau_n + \Delta T_p), \end{cases} \tag{10}$$
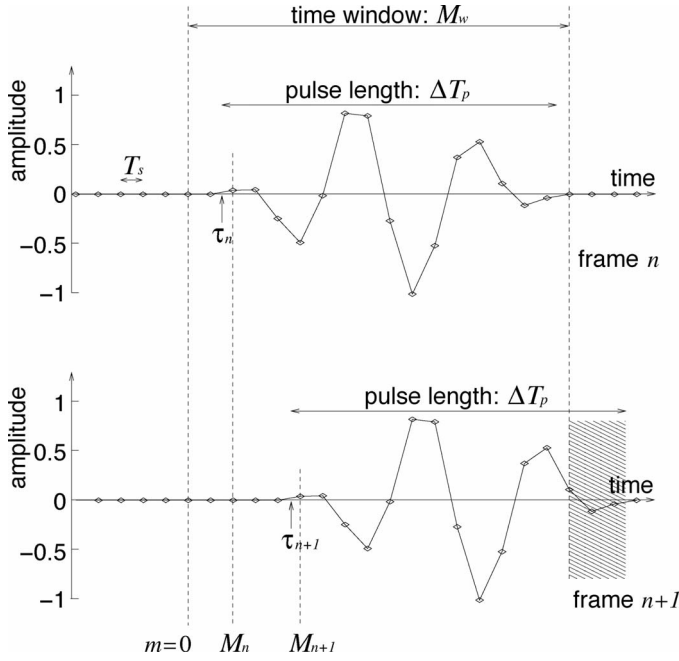

Fig. 1. Illustration of the change in relative position between the RF echo and the time window due to object displacement using simulated RF echoes.

because dominant echoes are reflected from two interfaces (lumen-intima and media-adventitia interfaces) [23] and because the distance between these interfaces is greater than the pulse duration. The distance between these interfaces is greater than 0.5 mm for carotid arteries, and the duration of the ultrasonic pulse used in this paper is about 0.25 μs, which corresponds to 385 μm in the case of a sound speed of 1540 m/s. Although a more complex model also should be investigated, the error source described in this paper influences even such a simple model. Therefore, a simple model was considered in this study to show an error source in estimation of the time shift of RF echoes.

III. RESULTS OF SIMULATION EXPERIMENTS

A. Power Spectrum of RF Echo Reflected from Carotid Artery

Fig. 2(a) shows an ultrasonic pulse of the diagnostic equipment used measured by a hydrophone placed in a

water tank. The hydrophone was placed at a distance of 20 mm from the surface of a linear-type probe, which corresponds to the electric focal depth. The signal received by the hydrophone was acquired at a sampling frequency of 1 GHz with a digital oscilloscope. The nominal center frequency of the linear-type ultrasonic probe used was 10 MHz.

An echo is expressed by the product of a sinusoidal wave at a center frequency, f_0, and an envelope, env(t), in the time domain. The frequency spectrum of a sinusoidal wave at frequency f_0 is expressed by a delta function, $\delta(f - f_0)$, in the frequency domain. Therefore, the frequency spectrum of an echo is a convolution of the spectrum, $S_{\mathrm{env}}(f)$, of the envelope and the delta function, $\delta(f - f_0)$, that shows the shifted version, $S_{\mathrm{env}}(f - f_0)$, of the spectrum of the envelope. When an envelope of an echo is expressed by functions such as a Hanning window or a Gaussian function, its power spectrum, $|S_{\mathrm{env}}(f)|^2$, becomes maximum at $f = 0$. Therefore, we can determine the actual center frequency by referring to the power spectrum of the echo, $|S_{\mathrm{env}}(f - f_0)|^2$, because $|S_{\mathrm{env}}(f - f_0)|^2$ becomes maximum at $f = f_0$.

As shown in Fig. 2(a), the envelope of the ultrasonic pulse has a finite duration of ΔT_p, that is, the sampled version of the envelope, env(m), is limited from $m = 0$ to $m = M_p$ (M_p: number of samples in the duration of the pulse). Therefore, a period that corresponds to the duration of the pulse is sufficient for the length of the time window for the Fourier transform. However, for example, the time window of 0.5 μs, which is sufficient for echoes in this paper, gives a sampling rate of $1/(0.5\ \mu s) = 2$ MHz for the frequency spectrum estimated by the discrete Fourier transform. To overcome such a low resolution of a frequency spectrum, $(M_0 - M_p)$ zero points are added to the time sequence extracted by the time window before application of the discrete Fourier transform. The estimated frequency spectrum is not changed by adding zero points as explained below. The time sequences $y(m)$ and $y'(m)$, with and without zero points, respectively, are equivalent to the time functions $y(t)$ and $y'(t)$, expressed as follows:

$$y(t) = \mathrm{env}(t)\ (0 \le t \le \Delta T_p), \tag{11}$$

$$y'(t) = \begin{cases} \mathrm{env}(t)\ (0 \le t \le \Delta T_p), \\ 0\ (\Delta T_p < t \le T_0), \end{cases} \tag{12}$$
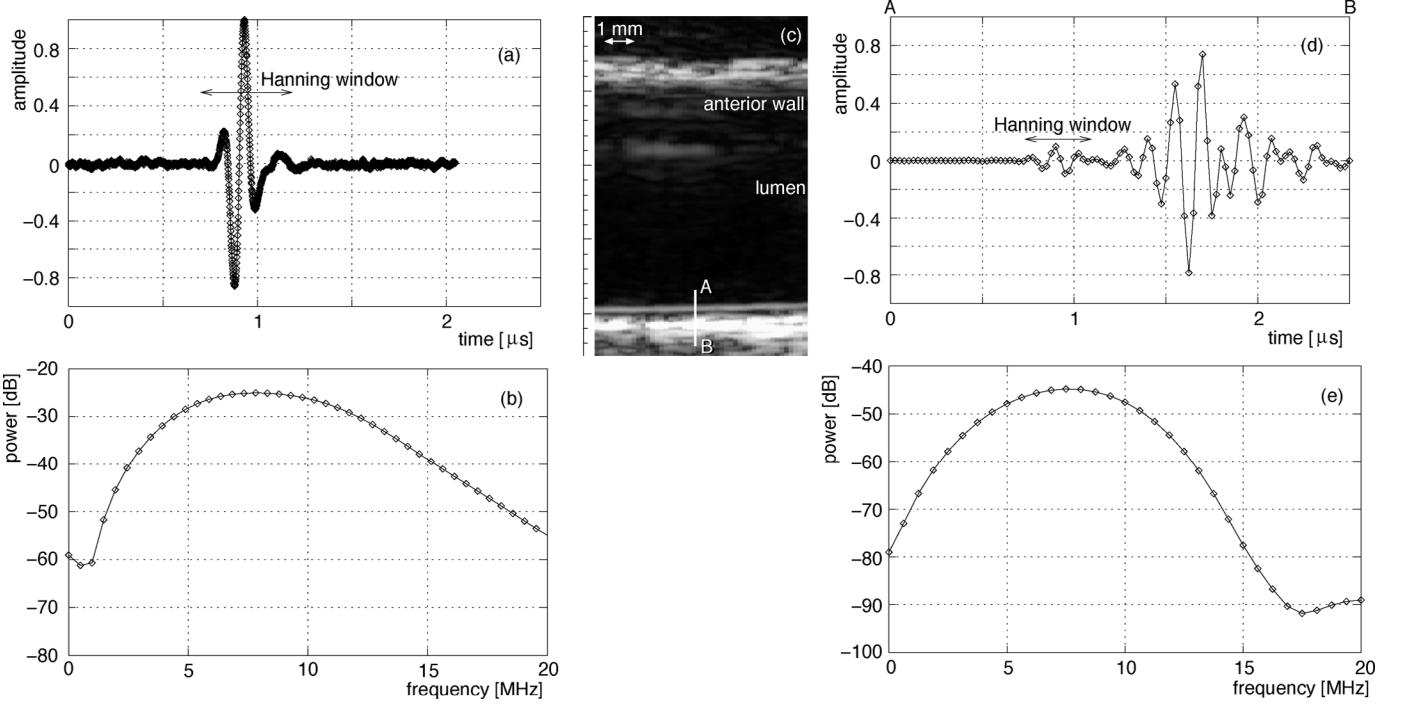
Fig. 2. Ultrasonic pulse of the diagnostic equipment used. (a) Ultrasonic pulse received by a hydrophone placed in a water tank (sampling frequency, 1 GHz). (b) Power spectrum of (a). (c) B-mode image of a human carotid artery. (d) RF echo from the posterior wall along the white vertical line shown in (c) (sampling frequency, 40 MHz). (e) Power spectrum (d).

where $T_0 = M_0 T_s$. There is no difference between the spectra $Y(f)$ and $Y'(f)$ of the time functions $y(t)$ and $y'(t)$:

$$Y'(f) = \int_{-\infty}^{\infty} y'(t) \cdot e^{-j2\pi ft} dt \qquad (13)$$
$$= \int_{0}^{\Delta T_p} \text{env}(t) \cdot e^{-j2\pi ft} dt = Y(f).$$

Therefore, no distortion occurs by the addition of zero points, and only the sampling rate of the spectrum, $Y(f)$ ($f = k/(M_0 T_s)$ ($k = 0, \ldots, M_0 - 1$)), obtained by the discrete Fourier transform is improved from $1/(MT_s)$ to $1/(M_0 T_s)$.

The sampled version of the frequency spectrum, $S_{\text{env}}(k)$, of the envelope is obtained from the convolution of $Y(k)$ with the frequency spectrum of the Hanning window used in the discrete Fourier transform.

A Hanning window with a length of 0.5 μs (512 points) was applied to the data set shown in Fig. 2(a) to extract a time sequence, and 1536 zero points were added. The power spectrum then was obtained by applying the Fourier transform as shown in Fig. 2(b). The power spectrum was found to have the largest value at about 8 MHz. In Fig. 2(b), the power spectrum at 20 MHz is sufficiently smaller (-30 dB) than that at the actual center frequency of 8 MHz. Therefore, the sampling frequency of 40 MHz of the ultrasonic diagnostic equipment used in this paper is sufficient for measuring RF echoes.

Fig. 2(c) shows the B-mode image of a human carotid artery. Along the white vertical line shown in Fig. 2(c), RF echoes reflected from the posterior wall were received as shown in Fig. 2(d) by the ultrasonic probe, which both

transmits ultrasound and receives echoes (sampling frequency: 40 MHz). Fig. 2(e) shows the power spectrum of the RF echo reflected from the lumen-intima interface, which was obtained from the time sequence (16 points = 0.4 μs) extracted by a Hanning window at the position shown in Fig. 2(d). Before application of the Fourier transform, 48 zero points were added. In Fig. 2(e), it can be seen that the center frequency was slightly changed to 7.5 MHz due to the frequency-dependent attenuation in tissue. Based on these results, the center frequency of the simulated RF echo is set at 7.5 MHz in the following section.

B. Simulated RF Echo

Fig. 3 shows the simulated RF echos, $\text{rf}_1(m)$ and $\text{rf}_2(m)$, at the 1st and 2nd frames based on (9) (center frequency: 7.5 MHz; 3 wavelength; envelope: Hanning window). The sampling frequency was set at 40 MHz. $\text{rf}_2(m)$ was shifted by 12.5 ns in comparison with $\text{rf}_1(m)$ due to object displacement. This time shift corresponds to a displacement of 9.625 μm and a velocity of 2.753 mm/s at a sound speed of 1540 m/s and a frame rate of 286 Hz. Typical velocity of the human carotid arterial wall is less than 10 mm/s. Therefore, the phase shifts between $\text{rf}_1(m)$ and $\text{rf}_2(m)$ were estimated for the cases of $\tau_2 - \tau_1 = 12.5$ ns (2.753 mm/s), 25 ns (5.506 mm/s), and 37.5 ns (8.258 mm/s) in the following section.

C. Estimation of Phase Shift of RF Echoes by Discrete Fourier Transform with a Hanning Window

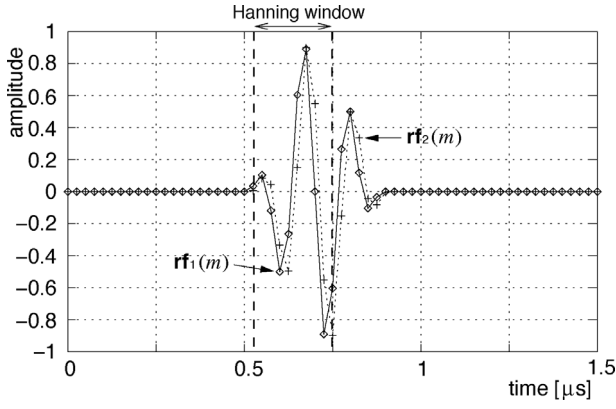Fig. 4(a) shows the signals after application of a Hanning window (length M_w: 10 points = 0.25 μs) to RF

Fig. 3. Simulated RF echoes, $rf_1(m)$ and $rf_2(m)$, based on (9). The time delay of $rf_2(m)$ from $rf_1(m)$ is 12.5 ns. The limits of the Hanning window are indicated by vertical dashed lines.
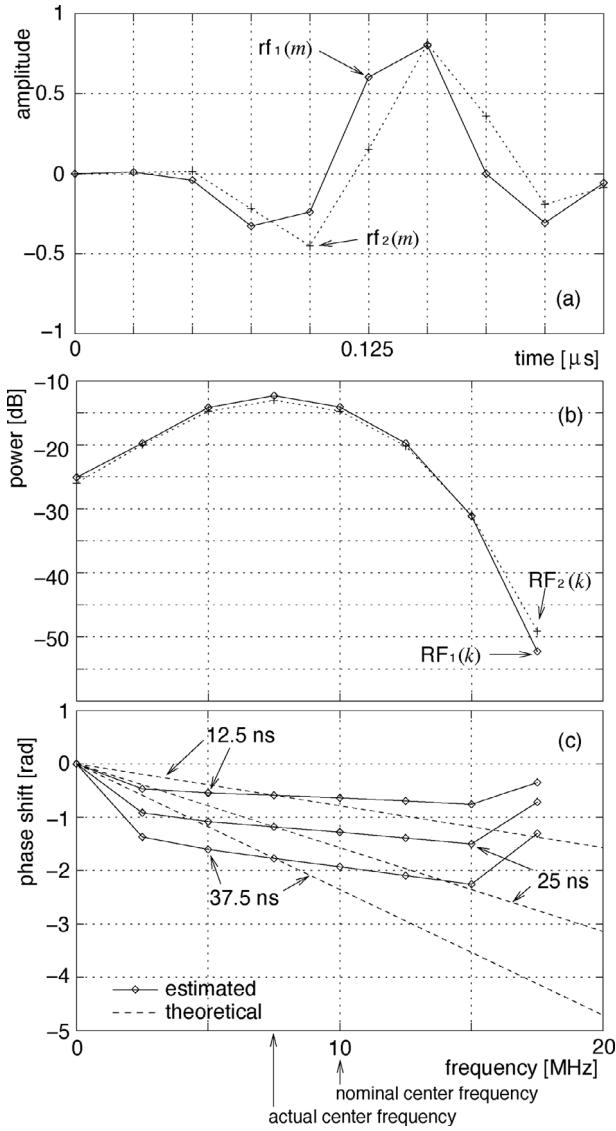

Fig. 4. (a) Signals after application of a Hanning window [0.25 μs (= 10 points)] to RF echoes shown in Fig. 3 ($\tau_2 - \tau_1 = 12.5$ ns). (b) Power spectra, $|RF_1(k)|$ and $|RF_2(k)|$, of $rf_1(m)$ and $rf_2(m)$ ($\tau_2 - \tau_1 = 12.5$ ns). (c) Phases of cross spectra, $\{RF_1(k)\}^* \cdot RF_2(k)$, for the cases of $\tau_2 - \tau_1 = 12.5$ ns, 25 ns, and 37.5 ns. The dashed line shows $-2\pi f(\tau_2 - \tau_1)$ for each case of $\tau_2 - \tau_1$.

echoes, $rf_1(m)$ and $rf_2(m)$, as shown in Fig. 3 (difference between time delays $\tau_2 - \tau_1$: 12.5 ns). By applying the Fourier transform, power spectra, $|RF_1(k)|$ and $|RF_2(k)|$, at a frequency $f = k/(M_w \cdot T_s)$ were obtained as shown in Fig. 4(b). Fig. 4(c) shows the phases of the cross-spectra, $\{RF_1(k)\}^* \cdot RF_2(k)$, and the dashed lines show $-2\pi f(\tau_2 - \tau_1)$ for the cases of $\tau_2 - \tau_1 = 12.5$ ns, 25 ns, and 37.5 ns.

In Fig. 4(c), it is found that the phase shift estimated at the nominal center frequency of 10 MHz is biased from $-2\pi f(\tau_2 - \tau_1)$. However, the change in time delay, $\tau_2 - \tau_1$, can be estimated precisely at the actual center frequency of 7.5 MHz. Therefore, the actual center frequency should be determined by referring to the power spectrum of the received RF echo, and the phase shift should be estimated at the actual center frequency.

The magnitude, $\Delta\tau_{\max}$, of the change in time delay is limited by half of the wavelength at the actual (selected) center frequency f_0 ($\Delta\tau_{\max} \leq 0.5/f_0$).

D. Considerations Regarding Error in Estimation of Change in Time Delay

For mathematical simplification, the envelope of an echo, $env_n(m)$, is assumed to be rectangular in this section. A Hanning window was used for the discrete Fourier transform.

1. Estimation of Change in Time Delay at a Frequency $f \neq f_0$: Frequency spectra, $RF_1(k)$ and $RF_2(k)$, at a frequency $f = k/(M_w \cdot T_s) \neq f_0$ of RF signals, $rf_1(m)$ and $rf_2(m)$, which are illustrated in Fig. 1, are obtained by applying the discrete Fourier transform with a Hanning window, $w(m)$, of M_w points as follows:

$$w(m) = \sin^2\left(2\pi \frac{mT_s}{M_w T_s}\right)$$
$$= \frac{1}{2} - \frac{e^{j2\pi \frac{mT_s}{M_w T_s}} + e^{-j2\pi \frac{mT_s}{M_w T_s}}}{4}. \quad (14)$$

$$RF_1(k) = \sum_{m=0}^{M_w-1} w(m) \cdot rf_1(m) \cdot e^{-j\omega m T_s}$$

$$= \sum_{m=M_1}^{M_w-1} w(m) \cdot rf_1(m) \cdot e^{-j\omega m T_s}$$

$$= \sum_{m=0}^{M_w-M_1-1} w(m+M_1) \cdot rf_1(m+M_1) \cdot e^{-j\omega(m+M_1)T_s}$$

$$= \frac{1}{2} \sum_{m=0}^{M_w-M_1-1} rf_1(m+M_1) \cdot e^{-j\omega(m+M_1)T_s}$$

$$- \frac{1}{4} \sum_{m=0}^{M_w-M_1-1} e^{j2\pi \frac{(m+M_1)T_s}{M_w T_s}} \cdot rf_1(m+M_1) \cdot e^{-j\omega(m+M_1)T_s}$$

$$- \frac{1}{4} \sum_{m=0}^{M_w-M_1-1} e^{-j2\pi \frac{(m+M_1)T_s}{M_w T_s}} \cdot rf_1(m+M_1) \cdot e^{-j\omega(m+M_1)T_s}$$

$$= A_1(k) - B_1(k) - C_1(k). \quad (15)$$

The first term, $A_1(k)$, in the right-hand side of (15), is rewritten as follows:

$$2 \cdot A_1(k) = \sum_{m=0}^{M_w-1} \mathrm{rf}_1(m) \cdot e^{-j\omega m T_s}$$

$$= \sum_{m=M_1}^{M_w-1} \mathrm{rf}_1(m) \cdot e^{-j\omega m T_s}$$

$$= \sum_{m=0}^{M_w-M_1-1} \mathrm{rf}_1(m+M_1) \cdot e^{-j\omega(m+M_1)T_s}$$

$$= \frac{1}{2j} \sum_{m=0}^{M_w-M_1-1} \left\{ e^{j\omega_0\{(m+M_1)T_s-\tau_1\}} \right.$$

$$\left. - e^{-j\omega_0\{(m+M_1)T_s-\tau_1\}} \right\} e^{-j\omega(m+M_1)T_s}$$

$$= \frac{1}{2j} e^{-j\omega_0\tau_1} \cdot e^{j(\omega_0-\omega)M_1 T_s} \sum_{m=0}^{M_w-M_1-1} e^{j(\omega_0-\omega)m T_s}$$

$$- \frac{1}{2j} e^{j\omega_0\tau_1} \cdot e^{-j(\omega_0+\omega)M_1 T_s} \sum_{m=0}^{M_w-M_1-1} e^{-j(\omega_0+\omega)m T_s}$$

$$= \frac{1}{2j} e^{-j\omega_0\tau_1} \cdot e^{j(\omega_0-\omega)M_1 T_s} \cdot \frac{1-e^{j(\omega_0-\omega)(M_w-M_1)T_s}}{1-e^{j(\omega_0-\omega)T_s}}$$

$$- \frac{1}{2j} e^{j\omega_0\tau_1} \cdot e^{-j(\omega_0+\omega)M_1 T_s} \cdot \frac{1-e^{-j(\omega_0+\omega)(M_w-M_1)T_s}}{1-e^{-j(\omega_0+\omega)T_s}}, \tag{16}$$

where $\omega = 2\pi k/(M_w \cdot T_s)$ and M_1 corresponds to the sampled point that is just after $t = \tau_1$. In the ultrasound system used, the sampling frequency, $1/T_s$, is equal to four times the nominal center frequency ($T_s \approx 1/(4f_0)$: f_0 is the actual center frequency). Therefore, the first term in the right-hand side of (16) is much larger than the second term because $\left|1-e^{j(\omega_0-\omega)T_s}\right| \ll 1$. Thus, (16) can be approximated as follows:

$$A_1(k) \approx \frac{1}{2} e^{-j\omega_0\tau_1} \cdot e^{j(\omega_0-\omega)M_1 T_s}$$

$$\cdot \frac{1-e^{j(\omega_0-\omega)(M_w-M_1)T_s}}{1-e^{j(\omega_0-\omega)T_s}}. \tag{17}$$

As well as $A(k)$, $B(k)$ and $C(k)$ are obtained as follows:

$$B_1(k) \approx \frac{1}{4} e^{-j\omega_0\tau_1} \cdot e^{j\left(\omega_0-\omega+\frac{2\pi}{M_w T_s}\right)M_1 T_s}$$

$$\cdot \frac{1-e^{j\left(\omega_0-\omega+\frac{2\pi}{M_w T_s}\right)(M_w-M_1)T_s}}{1-e^{j\left(\omega_0-\omega+\frac{2\pi}{M_w T_s}\right)T_s}}. \tag{18}$$

$$C_1(k) \approx \frac{1}{4} e^{-j\omega_0\tau_1} \cdot e^{j\left(\omega_0-\omega-\frac{2\pi}{M_w T_s}\right)M_1 T_s}$$

$$\cdot \frac{1-e^{j\left(\omega_0-\omega-\frac{2\pi}{M_w T_s}\right)(M_w-M_1)T_s}}{1-e^{j\left(\omega_0-\omega-\frac{2\pi}{M_w T_s}\right)T_s}}. \tag{19}$$

From (17), (18), and (19), (15) is expressed as follows:

$$\mathrm{RF}_1(k) \approx \frac{1}{2} e^{-j\omega_0\tau_1} \cdot e^{j(\omega_0-\omega)M_1 T_s}$$

$$\cdot \frac{1-e^{j(\omega_0-\omega)(M_w-M_1)T_s}}{1-e^{j(\omega_0-\omega)T_s}}$$

$$- \frac{1}{4} e^{-j\omega_0\tau_1} \cdot e^{j\left(\omega_0-\omega+\frac{2\pi}{M_w T_s}\right)M_1 T_s}$$

$$\cdot \frac{1-e^{j\left(\omega_0-\omega+\frac{2\pi}{M_w T_s}\right)(M_w-M_1)T_s}}{1-e^{j\left(\omega_0-\omega+\frac{2\pi}{M_w T_s}\right)T_s}} \tag{20}$$

$$- \frac{1}{4} e^{-j\omega_0\tau_1} \cdot e^{j\left(\omega_0-\omega-\frac{2\pi}{M_w T_s}\right)M_1 T_s}$$

$$\cdot \frac{1-e^{j\left(\omega_0-\omega-\frac{2\pi}{M_w T_s}\right)(M_w-M_1)T_s}}{1-e^{j\left(\omega_0-\omega-\frac{2\pi}{M_w T_s}\right)T_s}}.$$

As well as (20), $\mathrm{RF}_2(k)$ is obtained as follows:

$$\mathrm{RF}_2(k) \approx \frac{1}{2} e^{-j\omega_0\tau_2} \cdot e^{j(\omega_0-\omega)M_2 T_s}$$

$$\cdot \frac{1-e^{j(\omega_0-\omega)(M_w-M_2)T_s}}{1-e^{j(\omega_0-\omega)T_s}}$$

$$- \frac{1}{4} e^{-j\omega_0\tau_2} \cdot e^{j\left(\omega_0-\omega+\frac{2\pi}{M_w T_s}\right)M_2 T_s}$$

$$\cdot \frac{1-e^{j\left(\omega_0-\omega+\frac{2\pi}{M_w T_s}\right)(M_w-M_2)T_s}}{1-e^{j\left(\omega_0-\omega+\frac{2\pi}{M_w T_s}\right)T_s}} \tag{21}$$

$$- \frac{1}{4} e^{-j\omega_0\tau_2} \cdot e^{j\left(\omega_0-\omega-\frac{2\pi}{M_w T_s}\right)M_2 T_s}$$

$$\cdot \frac{1-e^{j\left(\omega_0-\omega-\frac{2\pi}{M_w T_s}\right)(M_w-M_2)T_s}}{1-e^{j\left(\omega_0-\omega-\frac{2\pi}{M_w T_s}\right)T_s}}$$

where M_2 corresponds to the sampled point that is just after $t = \tau_2$.

As shown in (20) and (21), in this case, the phase of $\{\mathrm{RF}_1(k)\}^* \cdot \mathrm{RF}_2(k)$ does not only depend on the change in time delay, $\tau_2 - \tau_1$.

2. Estimation of Change in Time Delay at the Center Frequency $f = f_0$: By assuming that a discrete frequency, $f = k_0/(M_w \cdot T_s)$, is identical to the actual center frequency, f_0, of the received RF echo, the frequency spectra, $\mathrm{RF}_1(k_0)$ and $\mathrm{RF}_2(k_0)$, of the RF signals, $\mathrm{rf}_1(m)$ and $\mathrm{rf}_2(m)$, are obtained by substituting $f = k_0/(M_w \cdot T_s) = f_0$ into (15). $A_1(k_0)$ is obtained as follows:

$$2 \cdot A_1(k_0) = \frac{1}{2j} e^{-j\omega_0\tau_1} \sum_{m=0}^{M_w-M_1-1} 1 - \frac{1}{2j} e^{j\omega_0\tau_1}$$

$$\cdot e^{-j2\omega_0 M_1 T_s} \sum_{m=0}^{M_w-M_1-1} e^{-j2\omega_0 m T_s}$$

$$= \frac{1}{2j} \cdot (M_w - M_1) \cdot e^{-j\omega_0\tau_1} - \frac{1}{2j} e^{j\omega_0\tau_1} \tag{22}$$

$$\cdot e^{-j2\omega_0 M_1 T_s} \frac{1-e^{-j2\omega_0(M_w-M_1)T_s}}{1-e^{-j2\omega_0 T_s}}.$$

When the time window is sufficiently long ($M_w \gg 1$), the second term in the right-hand side of (22) can be neglected:

$$A_1(k_0) \approx \frac{1}{4j} \cdot (M_w - M_1) \cdot e^{-j\omega_0\tau_1}. \qquad (23)$$

$B_1(k_0)$ is obtained as follows:

$$4 \cdot B_1(k_0) = \frac{1}{2j}e^{-j\omega_0\tau_1}\sum_{m=0}^{M_w-M_1-1}e^{j2\pi\frac{m+M_1}{M_w}} - \frac{1}{2j}e^{j\omega_0\tau_1}$$

$$\cdot e^{-j\left(2\omega_0+\frac{2\pi}{M_wT_s}\right)M_1T_s}\sum_{m=0}^{M_w-M_1-1}e^{-j\left(2\omega_0+\frac{2\pi}{M_wT_s}\right)mT_s}. \qquad (24)$$

As well as (22), the second term in the right-hand side of (24) can be neglected.

$$4 \cdot B_1(k_0) \approx \frac{1}{2j}e^{-j\omega_0\tau_1}\sum_{m=0}^{M_w-M_1-1}e^{j2\pi\frac{m+M_1}{M_w}}$$

$$= -\frac{1}{2j}e^{-j\omega_0\tau_1}\frac{1-e^{j2\pi\frac{M_1}{M_w}}}{1-e^{j\frac{2\pi}{M_w}}}. \qquad (25)$$

When the time window is properly applied to the echo (the difference between the beginnings of the window and the echo, which corresponds to M_1, is sufficiently small, that is, $M_1 \ll M_w$), $B(k_0) \approx 0$. As well as $B(k_0)$, $C(k_0) \approx 0$ under such a condition.

Therefore, $\mathrm{RF}_1(k_0)$, can be expressed as follows:

$$\mathrm{RF}_1(k_0) \approx \frac{1}{4j} \cdot (M_w - M_1) \cdot e^{-j\omega_0\tau_1}. \qquad (26)$$

As well as (26), $\mathrm{RF}_2(f_0)$ is obtained as follows:

$$\mathrm{RF}_2(k_0) \approx \frac{1}{4j} \cdot (M_w - M_2) \cdot e^{-j\omega_0\tau_2}. \qquad (27)$$

From (26) and (27):

$$\{\mathrm{RF}_1(k_0)\}^* \cdot \mathrm{RF}_2(k_0)$$

$$= -\frac{1}{16}(M_w - M_1)(M_w - M_2) \cdot e^{-j\omega_0(\tau_2-\tau_1)}. \qquad (28)$$

As shown in (28), the phase shift, which corresponds to the change in time delay, $\tau_2 - \tau_1$, can be estimated at the RF center frequency, $f_0 = k_0/(M_w \cdot T_s)$, even when the relative position between the RF echo and the time window is changed due to object displacement.

In Fig. 4(c), for example, the error in the estimated change in time delay at the nominal center frequency of 10 MHz is 2.3 ns in comparison with the true value of 12.5 ns, and it is not extremely large. Therefore, the measurement of velocity at a constant time (= depth) is not significantly influenced (for example, in blood flow measurement). However, to obtain the artery-wall displacement, the estimated velocity must be integrated with respect to time, and the error between each adjacent frame is accumulated. As shown in Fig. 4, the error described above
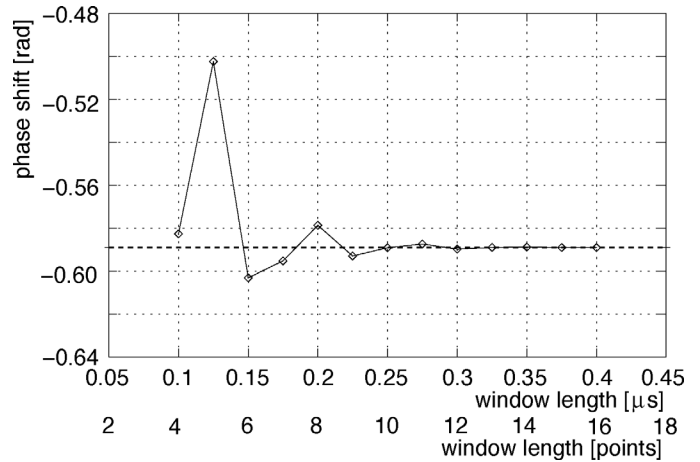

Fig. 5. Phase shift estimated at 7.5 MHz is plotted as a function of window length (with respect to simulated RF echoes, $\tau_2 - \tau_1 = 12.5$ ns).

depends on the magnitude of object displacement between two consecutive frames, i.e., magnitude of velocity. The velocity of the arterial wall is large during expansion and small during contraction. Therefore, the accumulated error in the displacement, which is obtained by integrating the estimated velocity, does not become zero. From these results, although a discrete frequency often does not exactly correspond to the actual center frequency, the phase shift should be estimated at the frequency that is the nearest to the actual center frequency to avoid the influence of the change in relative position between the RF echo and the time window.

E. Considerations Regarding Required Window Length

In Fig. 5, the phase of the cross spectra, $\{\mathrm{RF}_1(f_0)\}^* \cdot \mathrm{RF}_2(f_0)$, at the actual center frequency, f_0, which is obtained from the simulated RF echoes (f_0: 7.5 MHz, shown in Fig. 3), is plotted as a function of window length. The dashed line shows $2\pi f_0(\tau_2 - \tau_1)$. When the window length is less than 10 points (= 0.25 μs), the variation of the estimated phase shift is large. The Hanning window has a main lobe of $\pm 2/$(window length) in the frequency domain. When the frequency spectrum is estimated at the RF center frequency, f_0, the main lobe of the Hanning window ranges from $B_{w1} = f_0 - 2/$(window length) to $B_{w2} = f_0 + 2/$(window length). In the case of (window length) $< 2/f_0$, B_{w1} becomes less than zero, and the estimated frequency spectrum is influenced by the negative-frequency components. Therefore, the window length should be equal or greater than $2/f_0$. In Fig. 5, the window length of 0.25 μs (= 10 points) = $2/(8 \text{ MHz})$ almost corresponds to $2/f_0 = 2/(7.5 \text{ MHz})$.

In this paper, influences of random noise were not considered. The noise variance would be reduced using a longer time window. However, the window length is considered to be limited by the pulse duration. For example, when the window length is too long, both echoes from the lumen-intima and media-adventitia interfaces are included
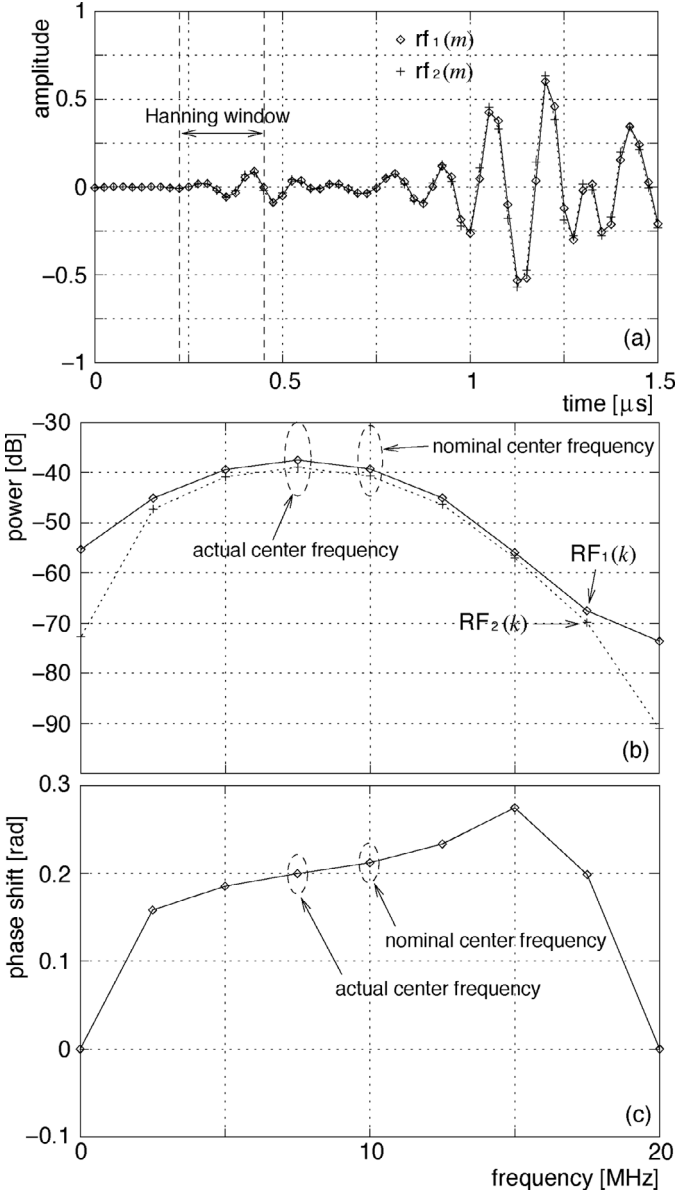
Fig. 6. (a) RF echoes reflected by the posterior wall of the human carotid artery. (b) Power spectra, $|\text{RF}_1(k)|$ and $|\text{RF}_2(k)|$, obtained by applying a Hanning window with a length of 0.25 μs = 10 points to waveforms shown in (a). (c) Phase of cross spectrum, $\{\text{RF}_1(k)\}^* \cdot \text{RF}_2(k)$.
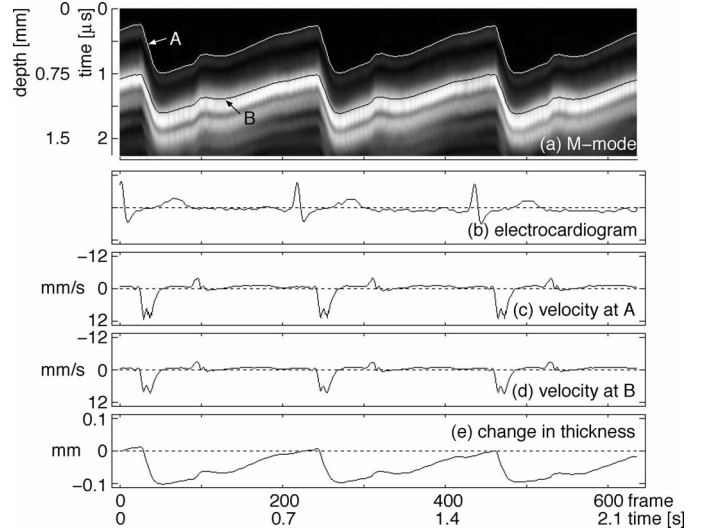

Fig. 7. In vivo experimental results for a carotid artery without atherosclerotic plaque (30-year-old healthy male). Change in thickness of the posterior wall due to the heartbeat estimated from the phase shift at 7.5 MHz. (a) M-mode image. (b) Electrocardiogram. (c) Velocity of the intimal side. (d) Velocity of the adventitial side. (e) Change in thickness of the posterior wall.

in the same time window. In this case, the noise variance would be reduced in comparison with a shorter time window. However, the change in time delay of the echo from the lumen-intima interface cannot be estimated because the estimated change in time delay is biased by that of the echo from the media-adventitia interface.

IV. In Vivo Measurement for Human Carotid Artery

Fig. 6(a) shows RF echoes reflected from the posterior wall of the carotid artery obtained at two consecutive frames (frame rate: 286 Hz). With respect to the echo

from the lumen-intima interface, the frequency spectrum was estimated with a Hanning window having a length of 0.25 μs = 10 points.

Fig. 6(b) shows the power spectra, $|\text{RF}_1(k)|$ and $|\text{RF}_2(k)|$, obtained by extracting the time sequences from $\text{rf}_1(m)$ and $\text{rf}_2(m)$ using the time window. From the estimated frequency spectra, $\text{RF}_1(k)$ and $\text{RF}_2(k)$, the phase shift between echoes was obtained from the phase of their cross-spectrum, $\{\text{RF}_1(k)\}^* \cdot \text{RF}_2(k)$, as shown in Fig. 6(c). The arterial wall then was tracked using the phase shifts estimated at both the nominal center frequency of 10 MHz and the actual center frequency of 7.5 MHz.

Figs. 7 and 8 show the results of artery-wall tracking using the phase shifts estimated at the actual center frequency of 7.5 MHz and the nominal center frequency of 10 MHz, respectively. Figs. 7(a) and (b) show the M-mode image and the electrocardiogram, respectively. The velocities shown in Figs. 7(c) and (d) were obtained at the intimal side and the adventitial side of the posterior wall, respectively. As shown in Figs. 7(a) and 8(a), the intimal side and the adventitial side were tracked by integrating the estimated velocities, $\widehat{v_n}$, of (7), and the tracked positions, $\widehat{d_{n+1}}$, of (8) were superimposed on M-mode images by a white line for the intimal side and a black line for the adventitial side. With respect to the intimal side, as shown in Fig. 8(a), an obvious tracking error was found when the phase shift was estimated at the nominal center frequency of 10 MHz. As for the adventitial side, the tracking error is not so obvious even at 10 MHz. However, the tracking shown by the black line is not in good agreement with the M-mode image in comparison with the result obtained at 7.5 MHz. For assessment of the relative elasticity, the change in wall thickness, which corresponds
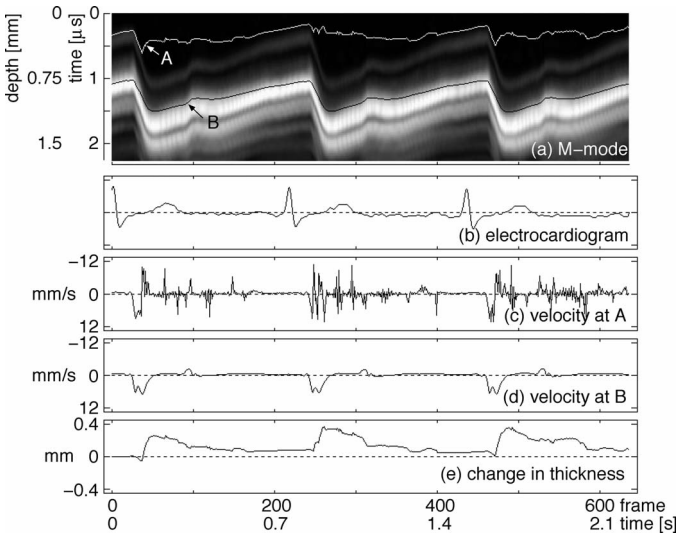
Fig. 8. In vivo experimental results for a carotid artery without atherosclerotic plaque (30-year-old healthy male). Change in thickness of the posterior wall due to the heartbeat estimated from the phase shifts at 10 MHz. (a) M-mode image. (b) Electrocardiogram. (c) Velocity of the intimal side. (d) Velocity of the adventitial side. (e) Change in thickness of the posterior wall.
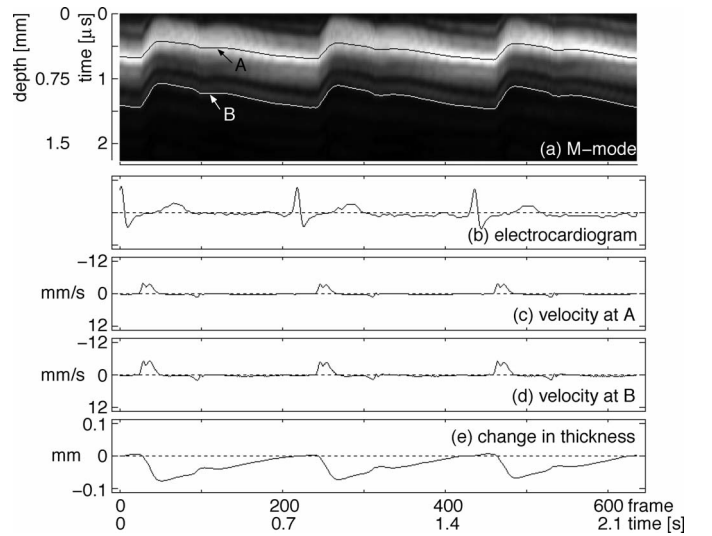

Fig. 9. In vivo experimental results for a carotid artery without atherosclerotic plaque (30-year-old healthy male). Change in thickness of the anterior wall due to the heartbeat estimated from the phase shift at 7.5 MHz. (a) M-mode image. (b) Electrocardiogram. (c) Velocity of the adventitial side. (d) Velocity of the intimal side. (e) Change in thickness of the anterior wall.

to the strain caused by the change in blood pressure, is obtained as shown in Fig. 7(e) [16], [17] from the difference between displacements at the intimal and adventitial sides. However, such a change in wall thickness as shown in Fig. 8(e), which was estimated at the nominal center frequency of 10 MHz, does not correspond to the wall strain (in cardiac systole, the artery diameter expands, and the wall thickness should become smaller). From these results, the phase-shift estimation at the actual center frequency was shown to be important even for the data sets measured for the human carotid artery.

The change in thickness would be dependent on the positions of points A and B, and thus changes in thickness were estimated at five different depths by shifting points A and B in the depth direction by 77 μm at a pitch of 19.25 μm. The distance between points A and B was kept constant. Mean and standard deviation of maximum changes in thickness during a heartbeat were estimated to be 97.6 μm and 6.9 μm. Slight influences of the positions of the assigned points were found. However, in cases of arteries with atherosclerotic plaque, there are many echoes in addition to those from the lumen-intima and media-adventitia interfaces. Under such a situation, the change in thickness would be more dependent on the position of the assigned points. Such a complex condition is not considered in this paper and should be investigated in a future work.

Fig. 9 shows the results of tracking in the anterior wall of the same subject as that shown in Fig. 7. The phase shift was estimated at 7.5 MHz. As in the case of the posterior wall, tracking was successfully performed for the anterior wall. A relatively smaller displacement was detected in comparison with that of the posterior wall.

V. Comparison with Autocorrelator Using Quadrature Demodulated Complex Signal

A correlation estimator with a quadrature demodulated complex signal is widely used for assessing artery-wall displacement. It is desirable that the demodulation frequency be the actual center frequency of the received RF echo because the problem mentioned below is the same as that already discussed.

In the quadrature demodulation, the received RF echo is multiplied by a complex sinusoidal function at a demodulation frequency, f_{dem}, as follows:

$$\mathrm{rf}_1(m) \cdot e^{j\omega_{dem}mT_s} = \frac{1}{2j}\Big\{e^{j\{(\omega_0+\omega_{dem})mT_s-\omega_0\tau_1\}}$$
$$- e^{-j\{(\omega_0-\omega_{dem})mT_s-\omega_0\tau_1\}}\Big\}, \quad (29)$$

$$\mathrm{rf}_2(m) \cdot e^{j\omega_{dem}mT_s} = \frac{1}{2j}\Big\{e^{j\{(\omega_0+\omega_{dem})mT_s-\omega_0\tau_2\}}$$
$$- e^{-j\{(\omega_0-\omega_{dem})mT_s-\omega_0\tau_2\}}\Big\}, \quad (30)$$

where $\omega_{dem} = 2\pi f_{dem}$.

When an ideal low-pass filter, $\mathrm{LPF}_{\mathrm{ideal}}[\cdot]$, is used, the quadrature demodulation gives the quadrature demodulated signals, $\check{\mathrm{rf}}_1(m)$ and $\check{\mathrm{rf}}_2(m)$, at a time, $t = mT_s$, as follows:

$$\check{\mathrm{rf}}_1(m) = \mathrm{LPF}_{\mathrm{ideal}}[\mathrm{rf}_1(m) \cdot e^{j\omega_{dem}mT_s}]$$
$$= -\frac{1}{2j}e^{-j\{(\omega_0-\omega_{dem})mT_s-\omega_0\tau_1\}}, \quad (31)$$

$$\check{\mathrm{rf}}_2(m) = \mathrm{LPF}_{\mathrm{ideal}}[\mathrm{rf}_2(m) \cdot e^{j\omega_{dem}mT_s}]$$
$$= -\frac{1}{2j}e^{-j\{(\omega_0-\omega_{dem})mT_s-\omega_0\tau_2\}}. \quad (32)$$

In this case, as described in [21], the phase of the 2-D autocorrelator, $r(m', n')$ (m': lag for the time (depth) axis, n': lag for the frame axis), with an $M \times N$ correlation window gives the phase shift, $\omega_0(\tau_2 - \tau_1)$, due to object displacement and the difference, $\omega_0 - \omega_{dem}$, between the demodulation frequency and the actual center frequency. For the simplest case ($M = N = 1$), to obtain object displacement at a depth that corresponds to $t = mT_s = 0$ (= the beginning of the time window as illustrated in Fig. 1), $r(0, 1)$ and $r(1, 0)$ are expressed using demodulated signals, $\check{\mathrm{rf}}_1(m)$ and $\check{\mathrm{rf}}_2(m)$, as follows:

$$
\begin{aligned}
r(0, n' = 1) &= \sum_{n=1}^{N=1} \check{\mathrm{rf}}_n^*(0) \cdot \check{\mathrm{rf}}_{n+n'}(0) \\
&= \check{\mathrm{rf}}_1^*(0) \cdot \check{\mathrm{rf}}_2(0) = \frac{1}{4} e^{j\omega_0(\tau_2 - \tau_1)},
\end{aligned}
\tag{33}
$$

$$
\begin{aligned}
r(m' = 1, 0) &= \sum_{m=1}^{M=1} \check{\mathrm{rf}}_1^*(m-1) \cdot \check{\mathrm{rf}}_1(m-1+m') \\
&= \check{\mathrm{rf}}_1^*(0) \cdot \check{\mathrm{rf}}_1(1) = \frac{1}{4} e^{j(\omega_{dem} - \omega_0)T_s}.
\end{aligned}
\tag{34}
$$

From the phase $\angle r(1, 0)$, the actual RF center frequency can be estimated as follows:

$$
\omega_{dem} - \frac{\angle r(1, 0)}{T_s} = \omega_0.
\tag{35}
$$

Therefore, the unbiased change in time delay, $\tau_2 - \tau_1$, which corresponds to object displacement, can be estimated as follows [22]:

$$
\tau_2 - \tau_1 = \frac{\angle r(0, 1)}{\omega_{dem} - \dfrac{\angle r(1, 0)}{T_s}}.
\tag{36}
$$

Next, let us consider a realistic case in which the moving average operator is used as a low-pass filter in the quadrature demodulation. The moving average estimator, $\mathrm{LPF}_{\mathrm{MA}}[\cdot]$, can be expressed as follows:

$$
\mathrm{LPF}_{\mathrm{MA}}[\cdot] = \frac{1}{M_w} \sum_{m=0}^{M_w - 1}.
\tag{37}
$$

Therefore:

$$
\begin{aligned}
\check{\mathrm{rf}}_1(0) &= \mathrm{LPF}_{\mathrm{MA}}[\mathrm{rf}_1(m) \cdot e^{j\omega_{dem} m T_s}] \\
&= \frac{1}{2j} \frac{1}{M_w} \sum_{m=0}^{M_w - 1} \left\{ e^{j\omega_0(mT_s - \tau_1)} \right. \\
&\quad \left. - e^{-j\omega_0(mT_s - \tau_1)} \right\} \cdot e^{j\omega_{dem} m T_s} \\
&= \frac{1}{2j} \frac{1}{M_w} \sum_{m=0}^{M_w - M_1 - 1} \left\{ e^{j\omega_0\{(m+M_1)T_s - \tau_1\}} \right. \\
&\quad \left. - e^{-j\omega_0\{(m+M_1)T_s - \tau_1\}} \right\} \cdot e^{j\omega_{dem}(m+M_1)T_s},
\end{aligned}
\tag{38}
$$

$$
\begin{aligned}
\check{\mathrm{rf}}_2(0) &= \mathrm{LPF}_{\mathrm{MA}}[\mathrm{rf}_2(m) \cdot e^{j\omega_{dem} m T_s}] \\
&= \frac{1}{2j} \frac{1}{M_w} \sum_{m=0}^{M_w - M_2 - 1} \left\{ e^{j\omega_0\{(m+M_2)T_s - \tau_2\}} \right. \\
&\quad \left. - e^{-j\omega_0\{(m+M_2)T_s - \tau_2\}} \right\} \cdot e^{j\omega_{dem}(m+M_2)T_s}.
\end{aligned}
\tag{39}
$$

It is found that $\check{\mathrm{rf}}_1(0)$ shown by (38) is identical to $A_1(k)$ at a frequency $f = k/(M_w \cdot T_s) = f_{dem}$ as shown by (16). Therefore, when $k/(M_w \cdot T_s) = f_{dem} \neq f_0$, the change in time delay, $\tau_2 - \tau_1$, cannot be estimated by (36) because $r(0, 1)$ corresponds to the cross spectrum, $\{\mathrm{RF}_1(k)\}^* \cdot \mathrm{RF}_2(k)$, and the phase of $\{\mathrm{RF}_1(k)\}^* \cdot \mathrm{RF}_2(k)$ does not give the change in time delay, $\tau_2 - \tau_1$, at a frequency other than the actual center frequency as described in Section III-D.

The 2-D autocorrelator gives the desirable results by (36) when $\mathrm{rf}_1(m)$ and $\mathrm{rf}_2(m)$ are stationary sinusoidal waves. If $\mathrm{rf}_1(m)$ and $\mathrm{rf}_2(m)$ are stationary sinusoidal waves at an angular frequency ω_0, $\check{\mathrm{rf}}_1(0)$ and $\check{\mathrm{rf}}_2(0)$ can be expressed as follows:

$$
\begin{aligned}
\check{\mathrm{rf}}_1(0) &= \frac{1}{2j} \frac{1}{M_w} \sum_{m=0}^{M_w - 1} \left\{ e^{j\{(\omega_0 + \omega_{dem})mT_s - \omega_0\tau_1\}} \right. \\
&\quad \left. - e^{-j\{(\omega_0 - \omega_{dem})mT_s - \omega_0\tau_1\}} \right\} \\
&\approx \frac{1}{2j} \frac{1}{M_w} e^{j\omega_0\tau_1} \cdot \frac{1 - e^{-j(\omega_0 - \omega_{dem})M_w T_s}}{1 - e^{-j(\omega_0 - \omega)T_s}},
\end{aligned}
\tag{40}
$$

$$
\begin{aligned}
\check{\mathrm{rf}}_2(0) &= \frac{1}{2j} \frac{1}{M_w} \sum_{m=0}^{M_w - 1} \left\{ e^{j\{(\omega_0 + \omega_{dem})mT_s - \omega_0\tau_2\}} \right. \\
&\quad \left. - e^{-j\{(\omega_0 - \omega_{dem})mT_s - \omega_0\tau_2\}} \right\} \\
&\approx \frac{1}{2j} \frac{1}{M_w} e^{j\omega_0\tau_2} \cdot \frac{1 - e^{-j(\omega_0 - \omega_{dem})M_w T_s}}{1 - e^{-j(\omega_0 - \omega)T_s}}.
\end{aligned}
\tag{41}
$$

The terms at the summed frequency, $\omega_0 + \omega_{dem}$, as well as (17), were neglected. Thus,

$$
\begin{aligned}
r(0, n' = 1) &= \sum_{n=1}^{N=1} \check{\mathrm{rf}}_n^*(0) \cdot \check{\mathrm{rf}}_{n+n'}(0) = \check{\mathrm{rf}}_1^*(0) \cdot \check{\mathrm{rf}}_2(0) \\
&= -\frac{1}{4M_w^2} \left| \frac{1 - e^{-j(\omega_0 - \omega)M_w T_s}}{1 - e^{-j(\omega_0 - \omega)T_s}} \right|^2 \cdot e^{j\omega_0(\tau_2 - \tau_1)},
\end{aligned}
\tag{42}
$$

$$
\begin{aligned}
r(m' = 1, 0) &= \sum_{m=1}^{M=1} \check{\mathrm{rf}}_1^*(m-1) \cdot \check{\mathrm{rf}}_1(m-1+m') \\
&= -\frac{1}{4M_w^2} \left| \frac{1 - e^{-j(\omega_0 - \omega)M_w T_s}}{1 - e^{-j(\omega_0 - \omega)T_s}} \right|^2 \cdot e^{j(\omega_0 - \omega_{dem})T_s}.
\end{aligned}
\tag{43}
$$

In this case, from (42) and (43), it is found that the change in time delay, $\tau_2 - \tau_1$, can be estimated by (36). From these facts, the 2-D autocorrelator is considered to be suitable for the narrow-band signal that can be considered as a continuous wave in an integration period of a low-pass filter.

Most conventional ultrasound systems use relatively narrowband ultrasonic pulses for the Doppler mode in comparison with that for the B-mode. Under the condition of a narrowband pulse and a high frame rate of several kilohertz, the 2-D autocorrelator provides precise results at a given demodulation frequency based on (36). However, a broadband pulse is preferable for improving the spatial resolution in displacement estimation. Under such a condition, the estimation should be performed at the center frequency of the received RF echo. In the case of an autocorrelator with quadrature demodulated signals, the demodulation frequency should be set at the center frequency of the RF echo.

VI. CONCLUSIONS

Digitized data of broadband RF echoes are available in modern ultrasonic diagnostic equipment. The phase shifts of RF echoes due to object displacement can be obtained at multiple frequencies by frequency analysis of RF echoes. This phase-shift estimation is influenced by the change in relative position of the RF echo in relation to the time window due to object displacement. Through simulations and in vivo experiments, this study showed that the phase shift should be estimated at the actual center frequency of an RF echo.

REFERENCES

[1] R. T. Lee, A. J. Grodzinsky, E. H. Frank, R. D. Kamm, and F. J. Schoen, "Structure-dependent dynamic mechanical behavior of fibrous caps from human atherosclerotic plaques," *Circulation*, vol. 83, pp. 1764–1770, 1991.

[2] H. M. Loree, A. J. Grodzinsky, S. Y. Park, L. J. Gibson, and R. T. Lee, "Static circumferential tangential modulus of human atherosclerotic tissue," *J. Biomech.*, vol. 27, pp. 195–204, 1994.

[3] M. Benthin, P. Dahl, R. Ruzicka, and K. Lindström, "Calculation of pulse-wave velocity using cross-correlation—Effects of reflexes in the arterial tree," *Ultrasound Med. Biol.*, vol. 17, no. 5, pp. 461–469, 1991.

[4] H. Kanai, K. Kawabe, M. Takano, R. Murata, N. Chubachi, and Y. Koiwa, "New method for evaluating local pulse wave velocity by measuring vibrations on aortic wall," *Electron. Lett.*, vol. 30, pp. 534–536, 1993.

[5] P. J. Brands, J. M. Willigers, L. A. F. Ledoux, R. S. Reneman, and A. P. G. Hoeks, "A noninvasive method to estimate pulse wave velocity in arteries locally by means of ultrasound," *Ultrasound Med. Biol.*, vol. 24, no. 9, pp. 1325–1335, 1998.

[6] A. Eriksson, E. Greiff, T. Loupas, M. Persson, and P. Pesque, "Arterial pulse wave velocity with tissue Doppler imaging," *Ultrasound Med. Biol.*, vol. 28, no. 5, pp. 571–580, 2002.

[7] J. M. Meinders, P. J. Brands, J. M. Willigers, L. Kornet, and A. P. G. Hoeks, "Assessment of the spatial homogeneity of artery dimension parameters with high frame rate 2-D B-mode," *Ultrasound Med. Biol.*, vol. 27, no. 6, pp. 785–794, 2001.

[8] A. P. G. Hoeks, C. J. Ruissen, P. Hick, and R. S. Reneman, "Transcutaneous detection of relative changes in artery diameter," *Ultrasound Med. Biol.*, vol. 11, no. 1, pp. 51–59, 1985.

[9] T. Länne, H. Stale, H. Bengtsson, D. Gustafsson, D. Bergqvist, B. Sonesson, H. Lecerof, and P. Dahl, "Noninvasive measurement of diameter changes in the distal abdominal aorta in man," *Ultrasound Med. Biol.*, vol. 18, no. 5, pp. 451–457, 1992.

[10] P. J. Brands, A. P. G. Hoeks, M. C. M. Rutten, and R. S. Reneman, "A noninvasive method to estimate arterial impedance by means of assessment of local diameter change and the local center-line blood flow velocity using ultrasound," *Ultrasound Med. Biol.*, vol. 22, no. 7, pp. 895–905, 1996.

[11] C. L. de Korte, E. I. Céspedes, A. F. W. van der Steen, and C. T. Lancée, "Intravascular elasticity imaging using ultrasound: Feasibility studies in phantoms," *Ultrasound Med. Biol.*, vol. 23, no. 5, pp. 735–746, 1997.

[12] E. I. Céspedes, C. L. de Korte, and A. F. W. van der Steen, "Intraluminal ultrasonic palpation: Assessment of local and cross-sectional tissue stiffness," *Ultrasound Med. Biol.*, vol. 26, no. 3, pp. 385–396, 2000.

[13] O. Bonnefous, "Blood flow and tissue motion with ultrasound for vascular applications," *Comptes Rendus de l'Acadmie des Sciences—Series IV—Physics*, vol. 2, no. 8, pp. 1161–1178, 2001.

[14] H. Kanai, M. Sato, Y. Koiwa, and N. Chubachi, "Transcutaneous measurement and spectrum analysis of heart wall vibrations," *IEEE Trans. Ultrason., Ferroelect., Freq. Contr.*, vol. 43, pp. 791–810, 1996.

[15] H. Kanai, H. Hasegawa, N. Chubachi, Y. Koiwa, and M. Tanaka, "Noninvasive evaluation of local myocardial thickening and its color-coded imaging," *IEEE Trans. Ultrason., Ferroelect., Freq. Contr.*, vol. 44, pp. 752–768, 1997.

[16] H. Kanai, Y. Koiwa, and J. Zhang, "Real-time measurements of local myocardium motion and arterial wall thickening," *IEEE Trans. Ultrason., Ferroelect., Freq. Contr.*, vol. 46, pp. 1229–1241, 1999.

[17] H. Hasegawa, H. Kanai, N. Hoshimiya, and Y. Koiwa, "Evaluating the regional elastic modulus of a cylindrical shell with nonuniform wall thickness," *J. Med. Ultrason.*, vol. 31, pp. 81–90, 2004.

[18] H. Kanai, H. Hasegawa, M. Ichiki, F. Tezuka, and Y. Koiwa, "Elasticity imaging of atheroma with transcutaneous ultrasound—Preliminary study," *Circulation*, vol. 107, pp. 3018–3021, 2003.

[19] C. Kasai, K. Namekawa, A. Koyano, and R. Omoto, "Real-time two-dimensional blood flow imaging using an autocorrelation technique," *IEEE Trans. Sonics Ultrason.*, vol. SU-32, pp. 458–464, 1985.

[20] T. Loupas and R. W. Gill, "Multifrequency Doppler: Improving the quality of spectral estimation by making full use of the information present in the backscattered RF echoes," *IEEE Trans. Ultrason., Ferroelect., Freq. Contr.*, vol. 41, no. 4, pp. 522–531, 1994.

[21] T. Loupas, J. T. Powers, and R. W. Gill, "An axial velocity estimator for ultrasound blood flow imaging, based on a full evaluation of the Doppler equation by means of a two-dimensional autocorrelation approach," *IEEE Trans. Ultrason., Ferroelect., Freq. Contr.*, vol. 42, no. 4, pp. 672–688, 1995.

[22] S. I. Rabben, S. Bjærum, V. Sørhus, and H. Torp, "Ultrasound-based vessel wall tracking: An auto-correlation technique with RF center frequency estimation," *Ultrasound Med. Biol.*, vol. 28, no. 4, pp. 507–517, 2002.

[23] A. D. M. van Swijndregt, S. H. K. The, E. J. Gussenhoven, C. T. Lancée, H. Rijsterborgh, E. Groot, A. F. W. van der Steen, N. Bom, and R. G. A. Ackerstaff, "An *in vitro* evaluation of the line pattern of the near and far walls of carotid arteries using B-mode ultrasound," *Ultrasound Med. Biol.*, vol. 22, no. 8, pp. 1007–1015, 1996.

Hideyuki Hasegawa was born in Oyama, Japan, in 1973. He received the B.E. degree from Tohoku University, Sendai, Japan, in 1996. He received the Ph.D. degree from Tohoku University in 2001. He is presently a research associate in Graduate School of Engineering, Tohoku University. His main research interest is medical ultrasound, especially diagnosis of atherosclerosis based on measurement of mechanical properties of the arterial wall. Dr. Hasegawa is a member of the IEEE, the Acoustical Society of Japan, the Japan Society of Ultrasonics in Medicine, and the Institute of Electronics, Information and Communication Engineers.

Hiroshi Kanai (M'98) was born in Matsumoto, Japan, on November 29, 1958. He received a B.E. degree from Tohoku University, Sendai, Japan in 1981, and M.E. and the Ph.D. degrees, also from Tohoku University, in 1983 and in 1986, both in electrical engineering.

From 1986 to 1988 he was with the Education Center for Information Processing, Tohoku University, as a research associate. From 1990 to 1992 he was a lecturer in the Department of Electrical Engineering, Faculty of Engineering, Tohoku University. From 1992 to 2001 he was an associate professor in the Department of Electrical Engineering, Faculty of Engineering, Tohoku University. Since 2001 he has been a professor in the Department of Electronic Engineering, Graduate School of Engineering, Tohoku University.

His present interests are in ultrasonic measurement and digital signal processing for diagnosis of heart diseases and arteriosclerosis.

Dr. Kanai is a member of the IEEE, the Acoustical Society of Japan, the Institute of Electronics Information and Communication Engineering of Japan, the Japan Society of Mechanical Engineers, the Japan Society of Ultrasonics in Medicine, the Japan Society of Medical Electronics and Biological Engineering, and the Japanese Circulation Society.